

12

AD A114013

# Reentry Vehicle Noretip Design for Minimum Total Heat Transfer

R. L. BAKER  
Vehicle Engineering Division  
and  
R. F. KRAMER  
Information Processing Division  
The Aerospace Corporation

15 April 1982

Final Report

APPROVED FOR PUBLIC RELEASE;  
DISTRIBUTION UNLIMITED

DTIC  
ELECTE  
APR 30 1982  
S D D

DTIC FILE COPY

Prepared for  
SPACE DIVISION  
AIR FORCE SYSTEMS COMMAND  
Los Angeles Air Force Station  
P.O. Box 92960, Worldway Postal Center  
Los Angeles, Calif. 90009

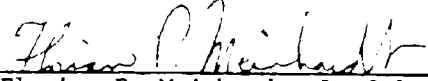
82 04 30 016

This interim report was submitted by The Aerospace Corporation, El Segundo, CA 90245, under Contract No. F04701-81-C 082 with the Space Division, Deputy for Technology, P.O. Box 92960, Worldway Postal Center, Los Angeles, CA 90009. It was reviewed and approved for The Aerospace Corporation by W. C. Riley, Director, Materials Sciences Laboratory. Lieutenant Eva L. Allen, SD/YLXT, was the project officer for the Mission Oriented Investigation and Experimentation (MOIE) Program.

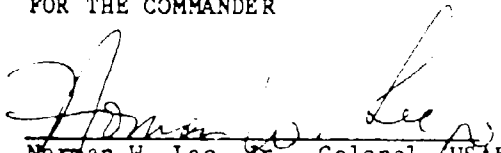
This report has been reviewed by the Public Affairs Office (PAS) and is releasable to the National Technical Information Service (NTIS). At NTIS, it will be available to the general public, including foreign nations.

This technical report has been reviewed and is approved for publication. Publication of this report does not constitute Air Force approval of the report's findings or conclusions. It is published only for the exchange and stimulation of ideas.

  
Eva L. Allen, 2nd Lt, USAF  
Project Officer

  
Florian P. Meinhardt, Lt Col, USAF  
Director of Advanced Space Development

FOR THE COMMANDER

  
Norman W. Lee, Sr., Colonel, USAF  
Deputy for Technology

UNCLASSIFIED

SECURITY CLASSIFICATION OF THIS PAGE (When Data Entered)

REPORT DOCUMENTATION PAGE		READ INSTRUCTIONS BEFORE COMPLETING FORM
1. REPORT NUMBER SD-TR-82-25	2. GOVT ACCESSION NO.	3. RECIPIENT'S CATALOG NUMBER
4. TITLE (and Subtitle) REENTRY VEHICLE NOSETIP DESIGN FOR MINIMUM TOTAL HEAT TRANSFER	5. TYPE OF REPORT & PERIOD COVERED Final	
	6. PERFORMING ORG. REPORT NUMBER TR-0082(9990)-1	
7. AUTHOR(s) R. L. Baker and R. F. Kramer	8. CONTRACT OR GRANT NUMBER(s) F04701-81-C-0082	
9. PERFORMING ORGANIZATION NAME AND ADDRESS The Aerospace Corporation El Segundo, California 90245		10. PROGRAM ELEMENT, PROJECT, TASK AREA & WORK UNIT NUMBERS
11. CONTROLLING OFFICE NAME AND ADDRESS Space Division Air Force Systems Command Los Angeles, Calif. 90009	12. REPORT DATE 15 April 1982	
	13. NUMBER OF PAGES 35	
14. MONITORING AGENCY NAME & ADDRESS (if different from Controlling Office)	15. SECURITY CLASS. (of this report) Unclassified	
	15a. DECLASSIFICATION/DOWNGRADING SCHEDULE	
16. DISTRIBUTION STATEMENT (of this Report)  Approved for public release; distribution unlimited.		
17. DISTRIBUTION STATEMENT (of the abstract entered in Block 20, if different from Report)		
18. SUPPLEMENTARY NOTES		
19. KEY WORDS (Continue on reverse side if necessary and identify by block number)  Nosetips Reentry vehicles Heat transfer		
20. ABSTRACT (Continue on reverse side if necessary and identify by block number)  A direct optimization method has been used to determine fixed fineness ratio nosetip shape contours for a specified vehicle ballistic coefficient and nosetip scale, which minimize the total trajectory nosetip laminar or turbulent heat transfer. These constraints neglect the interaction of the nosetip shape with vehicle performance characteristics. When this interaction is taken into account and additional new constraints of constant mass and volume are applied truncated cone nosetips are shown to result in the lowest total nosetip heat		

DD FORM 1473 (FACSIMILE)

UNCLASSIFIED  
SECURITY CLASSIFICATION OF THIS PAGE (When Data Entered)

UNCLASSIFIED

SECURITY CLASSIFICATION OF THIS PAGE(When Data Entered)

19. KEY WORDS (Continued)

20. ABSTRACT (Continued)

transfer. No attempt was made to optimize nosetip shape for the latter constraints.

UNCLASSIFIED

SECURITY CLASSIFICATION OF THIS PAGE(When Data Entered)

## ACKNOWLEDGMENTS

The vital assistance of Walter Reddall, III in providing the Godunov computer code results, Florence Tan in programming and running the optimization calculations and Maj. Kevin Yelmgren in reviewing the report is gratefully acknowledged.

Accession For	
NTIS GRA&I	<input checked="" type="checkbox"/>
DTIC TAB	<input type="checkbox"/>
Unannounced	<input type="checkbox"/>
Justification	
By _____	
Distribution/	
Availability Codes	
Dist	Avail and/or Special
A	





## CONTENTS

ACKNOWLEDGMENTS . . . . .	1
I. INTRODUCTION . . . . .	7
II. HEAT TRANSFER PREDICTION METHODS . . . . .	9
A. Integrated Heat Transfer Expressions . . . . .	9
B. Evaluation of $I_Q^L$ and $I_Q^T$ . . . . .	12
III. PROBLEM DEFINITION . . . . .	17
A. Mathematical Formulation . . . . .	17
B. Transversality Condition . . . . .	19
IV. RESULTS AND DISCUSSION . . . . .	21
A. Minimum Heat Transfer Nosedip Shapes . . . . .	21
B. Relative Heat Transfer Rates . . . . .	23
V. REENTRY VEHICLE APPLICATIONS . . . . .	27
A. Sphere-Cone Nosedips, Constant $m$ and $\beta$ . . . . .	27
B. Minimum Heat Transfer Nosedips, Constant $m$ , $\beta$ , and $V$ . . . . .	30
C. Truncated-Cone Nosedips, Constant $m$ , $\beta$ , and $V$ . . . . .	34
VI. SUMMARY AND CONCLUSIONS . . . . .	39

## FIGURES

1.	Laminar and Turbulent Heat Transfer Functions . . . . .	13
2.	Numerical Flowfield Calculation Methods . . . . .	15
3.	Minimum Heat Transfer Nosetip Shapes . . . . .	22
4.	Laminar and Turbulent $I_Q$ Values . . . . .	24
5.	Constant Ballistic Coefficient Reentry Vehicles . . . . .	29
6.	Nosetip Scaling Parameter for Sphere-cone and [ $I_Q^T$ ] <sub>min</sub> $\tau = 2$ Nosetips . . . . .	33
7.	Nosetip Scaling Parameters for Sphere-cone and Truncated Cone $\tau = 2$ Nosetips . . . . .	36

TABLES

1.	Calculated Heat Transfer and Drag Integrals . . . . .	25
2.	Calculated Noretip Heat Transfer and Drag Integrals . . . . .	35

## I. INTRODUCTION

Because the nosetip shape remains symmetric and unchanged throughout the trajectory, aerodynamic uncertainties for reentry vehicles with transpiration-cooled nosetips are considerably reduced. Present transpiration-cooled nosetip design shapes are sphere-cones. It is natural to ask if additional improvements in reentry vehicle performance could be achieved through the selection of alternate transpiration-cooled nosetip shapes. One such improvement might be a decrease in the amount of coolant required by the nosetip. In order to realize such a decrease, the total integrated heat transfer to the nosetip throughout a trajectory must be reduced.

The objective of this work has been to realistically examine the potential for decreasing reentry vehicle nosetip total heat transfer through the use of alternate nosetip shapes. In earlier work, Baker and Kramer<sup>1-3</sup> derived analytic expressions for nosetip and reentry vehicle total trajectory heat transfer. In Refs. 1 and 2 the dependence of total trajectory heat transfer on reentry parameters, nosetip or body scale, and geometry (shape) was derived and discussed. Then, in Ref. 3, this information was utilized and combined with classical variational calculus procedures and Newtonian pressure and velocity approximations to determine minimum heat transfer nosetip shapes.

---

<sup>1</sup> Baker, R. L. and R. F. Kramer, "Evaluation of Total Heat Transfer in Hypersonic Flow Environments," Report No. TR-0077(3550-15)-3, The Aerospace Corporation, El Segundo, California, August 1978.

<sup>2</sup> Baker, R. L. and R. F. Kramer, "Reentry Vehicle Total Heat Transfer for Fixed Weight and Ballistic Coefficient," The Aerospace Corporation, El Segundo, California (in preparation).

<sup>3</sup> Baker, R. L. and R. F. Kramer, "Nosetip Shape Optimization for Minimum Transpiration Coolant Requirements," Progress in Aeronautics and Astronautics, 59, 1978, pp. 404-427.

The present work improves upon the work of Ref. 3 by using inviscid flow field computer codes<sup>4, 5</sup> to compute the surface pressure distribution in place of the rough Newtonian approximations. The heat transfer minimization problem, in this study, is treated using direct optimization methods on flat-faced geometries.

In Section II, the required total heat transfer relationships are discussed. Then in Sections III and IV, the optimization problem to determine minimum heat transfer nosetip shapes for fixed vehicle ballistic coefficient, nosetip scale, and nosetip fineness ratio is defined, and the present results are compared with earlier approximate results. In Section V, consideration is given to the use of sphere-cone, minimum heat transfer, and truncated cone nosetips, with fixed fineness ratio, on conical reentry vehicles constrained to have specified mass, ballistic coefficient, and volume. These new constraints, which take into account the interaction of nosetip shape with vehicle performance characteristics, are shown to favor the use of truncated cone nosetips for achieving even lower total trajectory nosetip heat transfer. No attempt was made to optimize nosetip shape to achieve a minimum under these constraints.

---

<sup>4</sup>Masson, B. S., T. D. Taylor and R. M. Foster, "Application of Godunov's Method to Blunt Body Calculations," AIAA Journal, 7(4), 1969, p. 694.

<sup>5</sup>Baker, R. L., "Method of Characteristics Computer Program Including Embedded Shocks and Total Enthalpy Gradients Normal to Streamlines," Report No. TOR-0080(5550-01)-1, The Aerospace Corporation, San Bernardino, California, 31 January 1980.

## II. HEAT TRANSFER PREDICTION METHODS

### A. INTEGRATED HEAT TRANSFER EXPRESSIONS

When expressions for the laminar and turbulent convective heat-transfer coefficient given by Vaglio-Laurin<sup>6,7</sup> are used and the procedure of Allen and Eggers<sup>8</sup> is followed, the rate of change of integrated heat transfer with altitude  $dQ/dy$  is given by

$$\frac{dQ}{dy} = \frac{-C \rho_{\infty} V_{\infty}^2 \pi r_B^2}{Re_o^{n/n+1} \sin \theta_E} \int_0^{\bar{s}} \frac{\bar{\rho}_e \bar{u}_e \bar{\mu}_e \bar{r}^{n+1} d\bar{s}}{\left[ \int_0^{\bar{s}} \bar{\rho}_e \bar{u}_e \bar{\mu}_e \bar{r}^{n+1} d\bar{s} \right]^{n/n+1}} \quad (1)$$

where  $n = 1$  for laminar flow and  $n = 1/4$  for turbulent flow. When an integration in nondimensional surface distance  $\bar{s} = s/r_{\max}$  is performed, this expression becomes

$$\frac{dQ}{dy} = \frac{-(n+1)C \rho_{\infty} V_{\infty}^2 \pi r_B^2}{Re_o^{n/n+1} \sin \theta_E} I_Q^{1/n+1} \quad (2)$$

where the integral  $I_Q$  is given by

$$I_Q = \int_0^{\bar{s}} \bar{\rho}_e \bar{u}_e \bar{\mu}_e \bar{r}^{n+1} d\bar{s} \quad (3)$$

<sup>6</sup> Vaglio-Laurin, R., "Laminar Heat Transfer on Three-Dimensional Blunt Nosed Bodies in Hypersonic Flow," ARS Journal, 29, February 1959, pp. 123-129.

<sup>7</sup> Vaglio-Laurin, R., "Turbulent Heat Transfer on Blunt Nosed Bodies in Two-Dimensional and General Three-Dimensional Hypersonic Flow," J. Aero/Space Sciences, 27, January 1960, pp. 27-36.

<sup>8</sup> Allen, H. and A.J. Eggers, Jr., "A Study of the Motion and Aerodynamic Heating of Ballistic Missiles Entering the Earth's Atmosphere at High Supersonic Speeds," NACA Report 1381, 1958.

Allen and Eggers integrated an expression analogous to Eq. (2) representing  $\rho_{\infty}$  and  $V_{\infty}$  as functions of altitude  $y$  from their trajectory analysis and assuming  $Re_0$  to be constant. In the present analysis, the shock-layer Reynolds number  $Re_0 = [r_{\max} \sqrt{2H_0 \rho_0}] / \mu_0$  has also been represented as a function of altitude  $y$ .

Following the general integration procedure of Brunner<sup>9</sup>, the total heat transfer for an entire trajectory  $Q$  (Btu's) is obtained by integrating Eq. (2). The result for laminar flow is given by

$$Q^L = C_{fE}^L r_{\max}^{3/2} [\beta I_Q^L]^{1/2} \operatorname{erf}(\sqrt{B^L}) \quad (4)$$

and for turbulent flow by

$$Q^T = C_{fE}^T r_{\max}^{9/5} [\beta I_Q^T]^{4/5} \gamma [4/5, (B^T)^{4/5}] \quad (5)$$

The complete derivation of Eqs. (4) and (5) is given in Ref. 1. The  $\beta$  and  $r_{\max}$  in these equations are the vehicle ballistic coefficient ( $\text{lb}_m/\text{ft}^2$ ) and the maximum radial coordinate (ft) of the nosetip, respectively. The other parameters are given by

$$C^L = 1.866 \times 10^{-6} \left\{ \frac{[(\gamma+1)/(\gamma-1)]}{(2\omega+3)\lambda} \right\}^{1/2} \quad (6a)$$

$$C^T = \frac{4.70 \times 10^{-6}}{\lambda^{1/5}} \left\{ \frac{[(\gamma+1)/(\gamma-1)]}{(2\omega+9)} \right\}^{4/5} \quad (6b)$$

<sup>9</sup>Brunner, M. J., "Analysis of Aerodynamic Heating for a Re-entrant Space Vehicle," J. of Heat Transfer, 81, August 1959, pp. 223-229.

$$f_E^L = \frac{\mu_E^{1/2} V_E^{3/2}}{(\sin\theta_E)^{1/2}} \quad (7a)$$

$$f_E^T = \frac{\mu_E^{1/5} V_E^{9/5}}{(\sin\theta_E)^{1/5}} \quad (7b)$$

$$I_Q^L = \int_0^{\bar{s}} \bar{\rho}_e \bar{u}_e \bar{\mu}_e \bar{r}^2 d\bar{s} \quad (8a)$$

$$I_Q^T = \int_0^{\bar{s}} \bar{\rho}_e \bar{u}_e \bar{\mu}_e \bar{r}^{5/4} d\bar{s} \quad (8b)$$

$$B = [\rho^0 / (\lambda \beta \sin\theta_E)] \quad (9a)$$

$$B^L = [(2\omega+3)/4]B \quad (9b)$$

$$B^T = [(2\omega+9)/10]B \quad (9c)$$

The variables in these equations are the air specific heat ratio and viscosity law exponent  $\gamma$  and  $\omega$ , the density scale height factor in the exponential atmosphere  $\lambda$  (ft<sup>-1</sup>), the reentry velocity and entry flight path angle  $V_E$  (ft/sec) and  $\theta_E$ , the air viscosity evaluated at the entry stagnation temperature  $\mu_E$  (lb<sub>m</sub>/ft-sec), the ballistic factor  $B$ , the sea level air density  $\rho^0$  (lb<sub>m</sub>/ft<sup>3</sup>), and the nondimensional heat transfer integrals  $I_Q^L$  and  $I_Q^T$  which depend upon an integration in normalized surface running length of the local nondimensional boundary layer edge density  $\bar{\rho}_e = \rho_e / \rho_0$ , velocity  $\bar{u}_e = u_e / \sqrt{2H_0}$ , viscosity  $\bar{\mu}_e = \mu_e / \mu_0$ , and local normalized radial coordinate  $\bar{r} = r / r_{\max}$ . The functions

appearing in Eqs. (4) and (5) are the error function and the incomplete gamma function, respectively. These functions are given in terms of the appropriate laminar and turbulent modified ballistic factors  $B^L$  and  $B^T$  in Fig. 1.

It is now evident that if the reentry parameters  $V_E$  and  $\theta_E$ , vehicle ballistic coefficient  $\beta$ , and maximum nosetip radial coordinate  $r_{\max}$  are fixed, then the total laminar heat transfer  $Q^L$  will be minimized if we minimize the integral  $I_Q^L$ . Similarly, in the turbulent case,  $Q^T$  is minimized by minimizing the integral  $I_Q^T$ .

#### B. EVALUATION OF $I_Q^L$ AND $I_Q^T$

The heat transfer integrals  $I_Q^L$  and  $I_Q^T$ , given by Eqs. (8a) and (8b), respectively, depend only upon the nosetip geometry, i. e., upon the shape contour of the nosetip. The basic geometry considered in this and in earlier work is shown in the inset of Fig. 2. It consists of a nosetip having a flat face of height  $r(0)$ , to be determined, a maximum radial coordinate at the back  $r_{\max}$ , and a smoothly varying contour  $r = r(z)$  from the flat face expansion corner to the back of the nosetip. The flat face height  $r(0)$  is not constrained to be nonzero. Thus, the minimum heat transfer shape determined is not required to have a flat face. Note that the local nosetip coordinates  $r$  and  $z$  and the surface running length  $s$  are related to the local nosetip surface angle  $\alpha$  by the following simple trigonometric relationships:

$$\frac{dr}{dz} = \tan\alpha, \quad \frac{dr}{ds} = \sin\alpha \quad (10)$$

In Ref. 3, the local nondimensional boundary layer edge properties  $\bar{\rho}_e$ ,  $\bar{u}_e$ , and  $\bar{\mu}_e$  were represented as functions of  $\alpha$ , for  $\alpha < 90^\circ$ , by the simple hypersonic Newtonian approximations for pressure and velocity. Over the flat face portion of the nosetip,  $\alpha = 90^\circ$ , the product  $\bar{\rho}_e \bar{u}_e \bar{\mu}_e$  was assumed to vary linearly with the normalized distance to the sonic point at the expansion corner. In the present work, the flow pressure distributions were obtained numerically from accurate inviscid flow field calculation procedures.<sup>4, 5</sup>

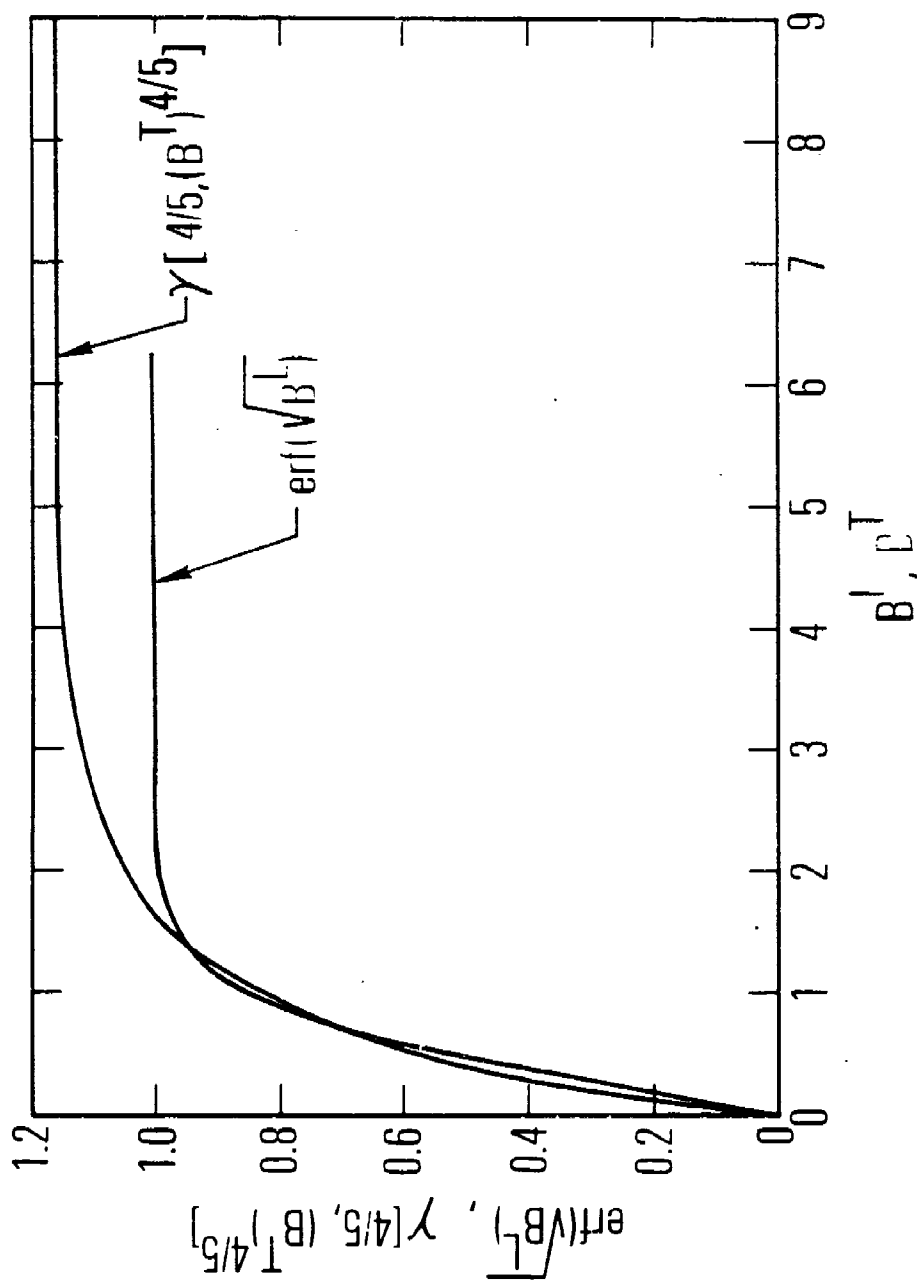


Fig. 1. Laminar and Turbulent Heat Transfer Functions

A schematic diagram illustrating the calculation procedure is shown in Fig. 2. The time-dependent (Godunov<sup>4</sup>) computer code required about 30 min of CDC 7600 computer run time to calculate the blunt body portion of the flat face flow field. However, it was only necessary to perform this calculation once, since this portion of the flow field does not depend upon  $r(0)/r_{\max}$  or upon the shape contour after the expansion corner. The supersonic portion of the flow field in all cases was calculated using a fast running rotational characteristics computer program<sup>5</sup> which required only two to three sec of computer time per specified flat face nosetip shape.

The normalized product  $\bar{\rho}_e \bar{\mu}_e$  can be written in terms of the normalized pressure  $\bar{p}_e = p_e/p_{t_2}$  as

$$\bar{\rho}_e \bar{\mu}_e = \frac{\rho_e \mu_e}{\rho_o \mu_o} = \bar{p}_e^{[(\gamma-1)\omega+1]/\gamma} \quad (11)$$

Also, assuming an isentropic expansion, the local nondimensional velocity  $\bar{u}_e$  can be written in terms of  $\bar{p}_e$  as

$$\bar{u}_e = \frac{u_e}{\sqrt{2H_o}} = \sqrt{1 - \bar{p}_e^{(\gamma-1)/\gamma}} \quad (12)$$

Thus,  $I_Q$  is a function of the specific heat ratio  $\gamma$ , the temperature exponent in the viscosity law  $\omega$ , and body geometry. In this work, the hypersonic values  $\gamma = 1.2$  and  $\omega = 1.0$  have been used throughout. The integrals  $I_Q^L$  and  $I_Q^T$  were calculated numerically from Eqs. (8a) and (8b) for specified geometry using the calculated surface pressure distribution for that geometry and Eqs. (11) and (12).

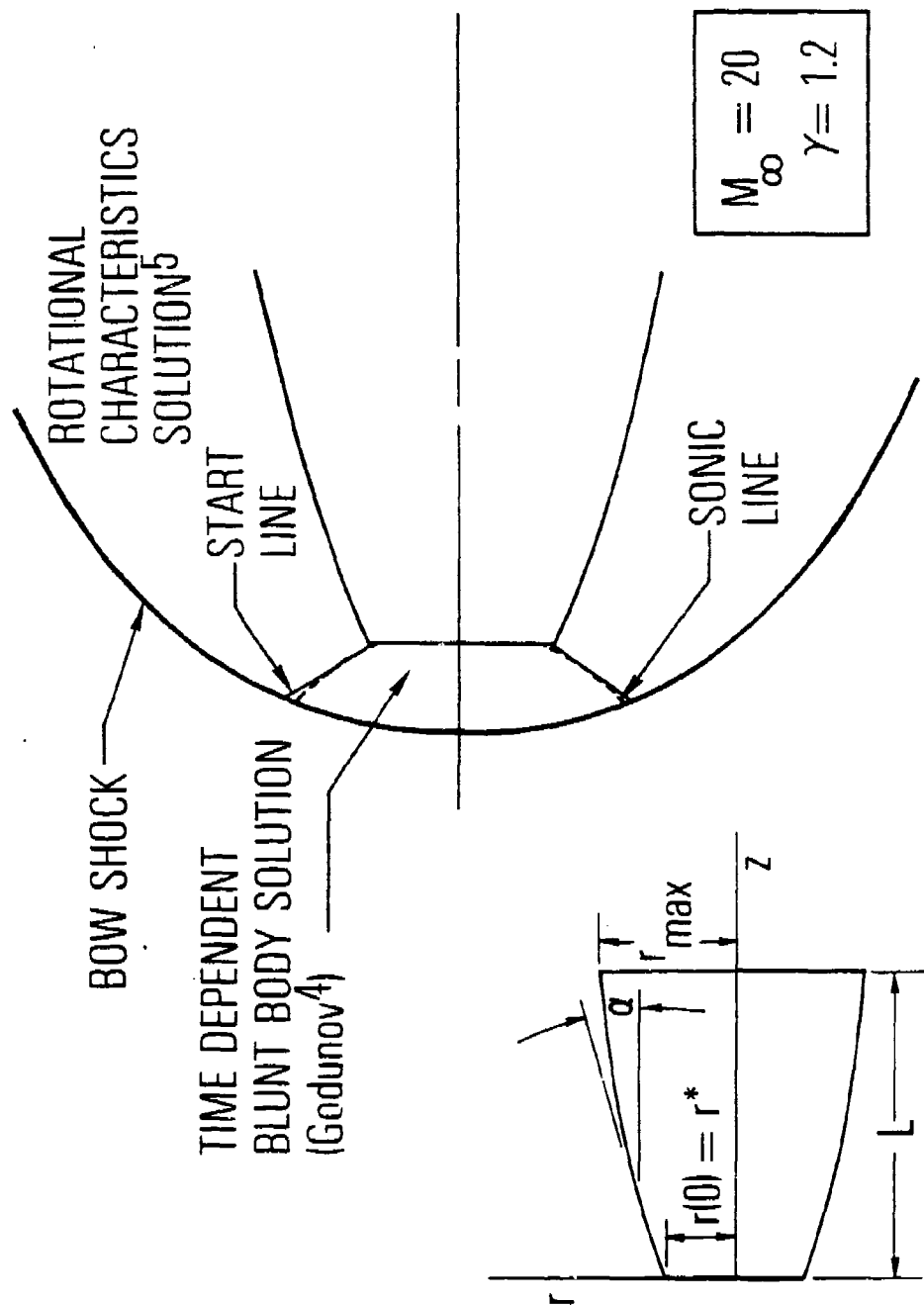


Fig. 2. Numerical Flowfield Calculation Methods

### III. PROBLEM DEFINITION

#### A. MATHEMATICAL FORMULATION

In this section, we will be concerned with the determination of those flat-faced shapes that produce minimum values of  $I_Q$ . Nosetip shapes with a flat forward face of unspecified height  $r^* = r(0)$  will be considered (see Fig. 2). Normalizing all coordinates by  $r_{\max}$  define

$$x = z/r_{\max}, \quad y = r/r_{\max} \quad (13)$$

Following the general procedures used in Ref. 3, the  $I_Q$  integrals given by Eqs. (8a) and (8b) may be expressed as

$$I_Q = [I_Q]_{\text{face}} + [I_Q]_{\text{nose}} \quad (14a)$$

$$= \frac{1}{n+2} y(0)^{n+2} + \int_0^{2/\pi} \frac{\bar{\rho}_e \bar{u}_e \bar{\mu}_e y^{n+1}}{\cos \alpha} dx \quad (14b)$$

where  $n = 1$  for laminar flow and  $n = 1/4$  for turbulent flow. The fineness ratio  $\tau = 2r_{\max}/L$  is to be specified.

The value of the parameter  $G$  defines the heat transfer to the flat face portion of the nosetip. The  $G$  for both laminar and turbulent flow was determined in the present work using calculated  $\bar{p}_e$  values from the finite element (time-dependent) flow field computer code<sup>4</sup>, evaluating  $\bar{\rho}_e \bar{\mu}_e$  and  $\bar{u}_e$  from Eqs. (11) and (12), respectively, and numerically integrating Eqs. (8a) and (8b). The calculated values of  $G$  are

$$G^L = 0.0375 \quad (15a)$$

$$G^T = 0.0449 \quad (15b)$$

Substituting Eqs. (11) and (12) into Eq. (14b), the functional to be minimized may be written in the following form:

$$I_Q = \frac{G}{n+2} y(0)^{n+2} = \int_0^{2/\tau} F(\alpha, \bar{p}_e, y) dx \quad (16)$$

Because of the coupling with the method-of-characteristics computer program<sup>5</sup> for evaluation of the integral in Eq. (16), it was decided not to attempt to derive an Euler equation corresponding to this variational problem as done in Ref. 3. Instead, a purely numerical minimization approach was used. The shape  $y(x)$  was approximated by a truncated Fourier series which satisfies the boundary conditions  $\dot{y}(0) = dy/dx(0) = b$  (constant  $b$  specified in Section III-B) and  $y(2/\tau) = 1$ .

$$y(x) = \left(1 - \frac{2b}{\tau}\right) + bx + \sum_{i=1}^N \alpha_i \cos \left[ \frac{2i-1}{2} \frac{\pi \tau x}{2} \right] \quad (17)$$

A nosetip shape is thus defined by specifying the  $N$  parameters  $\alpha_i$  ( $i=1, \dots, N$ ). For a given shape, the flow field may be found using the method of characteristics code. This determines  $\bar{p}_e$ ,  $\bar{u}_e$ , and  $\bar{\mu}_e$  along the body, through Eqs. (11) and (12), and the integral in Eq. (16) may then be evaluated. The variational problem has thus been replaced by the finite parameter minimization problem; minimize

$$I_Q(\alpha_1, \dots, \alpha_N). \quad (18)$$

This problem was solved iteratively using the Davidon-Fletcher-Powell Method.<sup>10</sup> It was determined that  $N = 3$  produced sufficient accuracy for the present calculations.

<sup>10</sup>Greenstadt, J., "Variations on Variable-Metric Methods," Math. of Comp. 24, 1970, pp. 1-22.

## B. TRANSVERSALITY CONDITION

Since  $y(0)$  is not specified, the minimization of the functional  $I_Q$ , as given by Eq. (16), is a variable end point problem of the calculus of variations, and the following transversality condition must be satisfied at  $x = 0$ .<sup>11</sup>

$$\frac{\partial F}{\partial \dot{y}} - G y(0)^{n+1} = 0 \quad (19)$$

The flow downstream from the expansion corner is supersonic, therefore, conditions at  $x = 0$  cannot be influenced by conditions downstream. Hence, the transversality condition Eq. (19) may be evaluated using the Prandtl-Meyer relations<sup>12</sup> to represent the flow variables as a function of flow angle through the corner expansion. This leads to the following expression for  $\partial F/\partial \dot{y}$ :

$$\frac{\partial F}{\partial \dot{y}} = \frac{y^{n+1} \left[ K_1 p_e^{[(\gamma-1)\omega+1]/\gamma} + K_2 p_e^{[(\gamma-1)\omega+1]/\gamma} \right]}{\sqrt{1 - p_e^{(\gamma-1)/\gamma}}} \quad (20)$$

where

$$K_1 = \sin \alpha + \left[ \frac{(\gamma-1)\omega+1}{\gamma} \right] \left[ \frac{\gamma M^2}{\sqrt{M^2-1}} \right] \cos \alpha \quad (21a)$$

$$K_2 = -\sin \alpha + \left[ \frac{2\omega-1-(2\omega+1)\gamma}{\gamma} \right] \left[ \frac{\gamma M^2}{\sqrt{M^2-1}} \right] \cos \alpha \quad (21b)$$

and  $M$  is the Mach number corresponding to the flow angle  $\alpha$  in the Prandtl-Meyer expansion.

<sup>11</sup> Miele, A. (ed.), "Theory of Optimum Aerodynamic Shapes," Applied Mathematics and Mechanics, 9, Academic Press, N. Y., 1965.

<sup>12</sup> Liepmann, H. W. and A. Roshko, Elements of Gasdynamics, John Wiley & Sons, Inc., N. Y. (1957), pp. 92-100.

If  $y(0) \neq 0$ , Eq. (19) may be divided by  $y(0)^{n+1}$ . Thereafter, substituting for  $\partial F / \partial \dot{y}$  from Eq. (20), the resulting equation is a nonlinear equation in  $\dot{y}(0)$ . The numerical solution of this equation yields the following values:

$$\dot{y}(0)^L = 0.3716 \quad (22a)$$

$$\dot{y}(0)^T = 0.3147 \quad (22b)$$

Equations (22a) and (22b) fix the slope of the minimum heat transfer nosetip shapes at  $x = 0$  for the laminar and turbulent cases, respectively. The angles corresponding to these slopes are  $20.39^\circ$  and  $17.47^\circ$ , respectively. The values of  $y(0)$  at  $x = 0$ , i. e., the flat face heights, are determined iteratively as part of the overall solution procedure described in the problem formulation discussion above.

#### IV. RESULTS AND DISCUSSION

Results obtained by use of the direct optimization methods discussed above are presented herein for the cases of both laminar and turbulent flow in the boundary layer. In all cases, the specific heat ratio  $\gamma$  and the viscosity law exponent  $\omega$  have been assumed to be the hypersonic values 1.2 and 1.0, respectively.

##### A. MINIMUM HEAT TRANSFER NOSETIP SHAPES

Calculated minimum laminar and turbulent heat transfer shapes for fineness ratios,  $\tau = 2r_{\max}/L$ , of 1, 2, 4 and 8 are shown in Fig. 3. The flat face height for the minimum heat transfer shape, determined in each case as part of the solution, decreases quite rapidly from a large fraction of  $r_{\max}$  for  $\tau = 8$  to 35% of  $r_{\max}$  for  $\tau = 1$ . In all cases, the  $r(0)$  is greater for the turbulent flow solution than for the laminar case with the same  $\tau$ . This is probably due to the smaller exponent of  $r(0)$  in the expression for  $[I_Q]_{\text{face}}$ , Eq. (14b), in the case of turbulent flow than in the case of laminar flow.

For comparison, the minimum heat transfer shapes calculated earlier in Ref. 3 using the Newtonian approximations are also shown in Fig. 3. In all cases, the flat face heights are greater than those for the present solutions. This is especially true for the  $\tau = 1$  case. The main reason for this is the larger flow angles at the expansion corner ( $17-20^\circ$  instead of  $3-4^\circ$ ), indicated by the present transversality condition using the Prandtl-Meyer equations in place of the Newtonian approximations. In the Newtonian approximation solutions, so little difference is predicted between the minimum heat transfer laminar and turbulent shapes for these  $\tau$  values that only one shape is shown. The Newtonian approximation solutions each have monotonically decreasing slopes after the expansion corner, whereas the present minimum heat transfer nosetip shapes are inflected for  $\tau \geq 2$ . A truncated sphere or a  $5^\circ$  sphere-cone shape is shown in each case for shape comparison purposes.

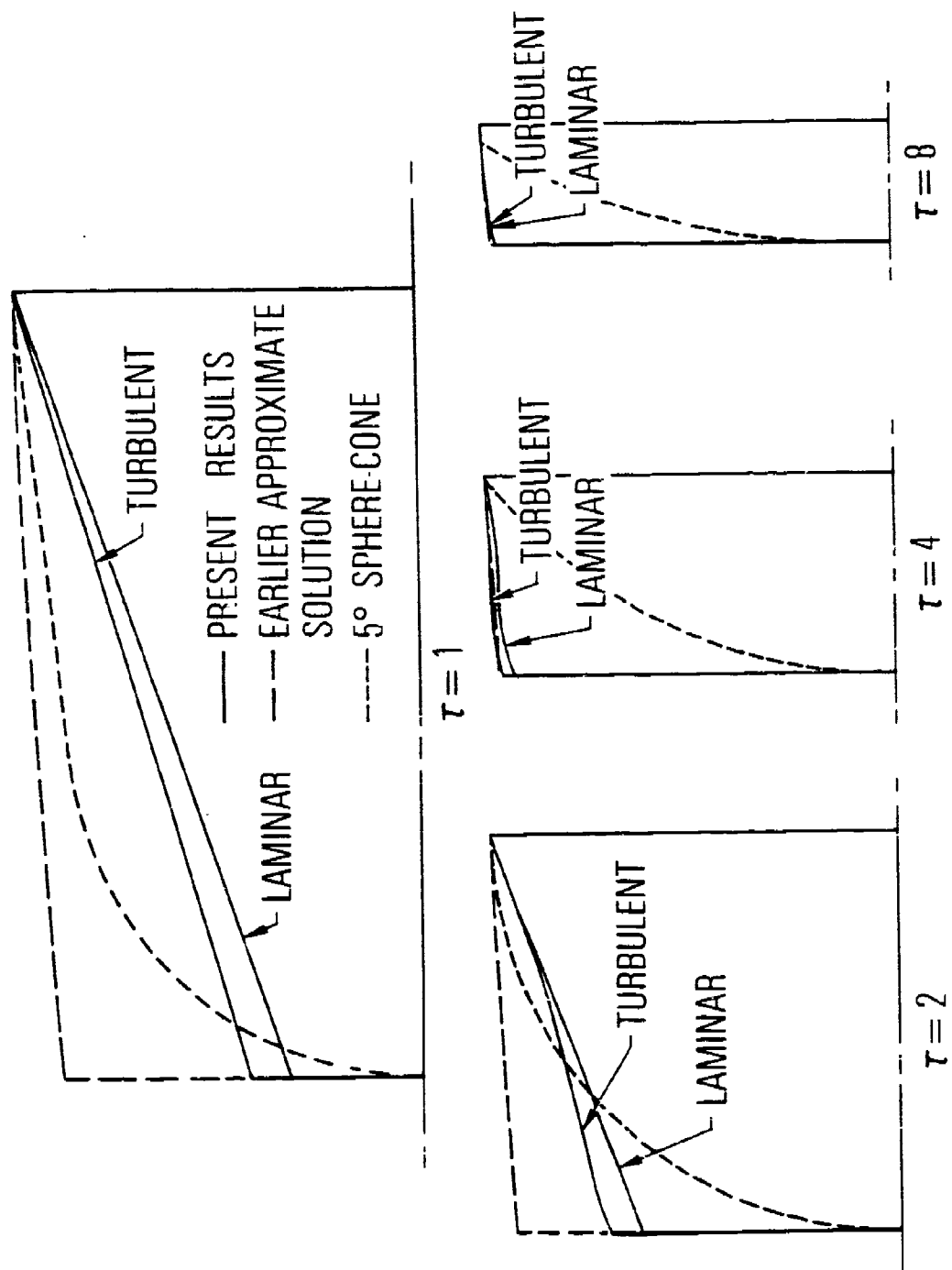


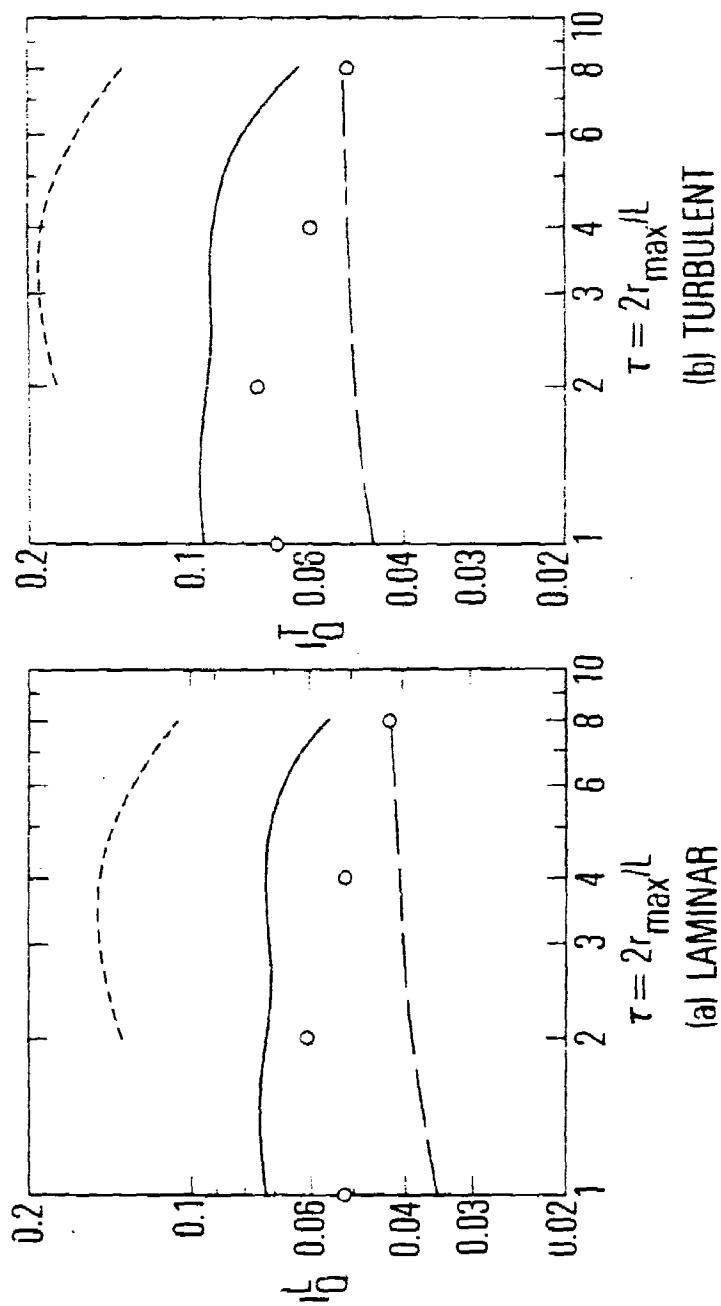
Fig. 3. Minimum Heat Transfer Nosetip Shapes

## B. RELATIVE HEAT TRANSFER RATES

Calculated minimum laminar and turbulent  $I_Q$  values for the shapes shown in Fig. 3 are given in Fig. 4. The earlier results, also shown, had indicated that the laminar and turbulent  $I_Q$  values for a minimum heat transfer nosetip shape were up to three to four times smaller than those for a truncated sphere having the same fineness ratio. The present results indicate calculated  $I_Q$  values for truncated spheres much lower than those of the earlier results and calculated minimum  $I_Q$  values higher than those indicated from the approximate calculations. Overall, this dictates that the potential reduction in heat transfer, obtained by employing a minimum heat transfer nosetip shape instead of a sphere-cone shape, is much less than predicted earlier.

The reasons for this behavior are related to the type of errors inherent in the Newtonian approximations. In general, the Newtonian velocity  $\bar{u}_e = \cos\alpha$  is as much as a factor of 2 too high, whereas the Newtonian pressure  $\bar{p}_e = \sin^2\alpha$  is reasonably accurate on the blunt portion of the nosetip ( $\alpha > 45$ ) and becomes even more than a factor of 2 too low for very small body angles ( $\alpha < 5$ ). In the results shown in Fig. 4, the velocity error tends to dominate in the spherical shape calculations, whereas the pressure error dominates in the minimum heat transfer shape predictions.

A comparison of the calculated numerical values of  $I_Q$  for the present minimum heat transfer shapes to those for truncated spheres or sphere-cones having the same fineness ratio  $\tau$  is shown in Table 1. The maximum reduction in  $I_Q$  is about 35%. As a matter of interest in later discussion, the values of the drag integral  $I_D$  for the various shapes are also shown.



- APPROXIMATE FLOWFIELD, TRUNCATED SPHERES
- .- APPROXIMATE FLOWFIELD, MINIMUM HEAT TRANSFER
- PRESENT RESULTS, TRUNCATED SPHERES AND SPHERE-CONES
- PRESENT RESULTS, MINIMUM HEAT TRANSFER

Fig. 4. Laminar and Turbulent  $I_Q$  Values

Table 1. Calculated Heat Transfer and Drag Integrals

$\tau$	5° Sphere-Cone		Minimum Heat Transfer			
			Laminar		Turbulent	
	$I_Q^L$	$I_Q^T$	$I_Q^L$	$I_D$	$I_Q^T$	$I_D$
1	0.0784	0.0999	0.0544	0.0912	0.0686	0.116
2	0.0734	0.0938	0.0612	0.227	0.0750	0.367
4	0.0724	0.0903	0.0513	0.413	0.0593	0.431
8	0.0550	0.0631	0.0423	0.433	0.0500	0.433

## V. REENTRY VEHICLE APPLICATIONS

The minimum heat transfer shapes determined in the previous sections were obtained assuming that the reentry conditions, ballistic coefficient  $\beta$ , and nosetip scale  $r_{\max}$  could be fixed independently. If we consider the interaction of  $\beta$  and  $r_{\max}$ , then these quantities can no longer be specified independently. In this section, sphere-cone reentry vehicles constrained to have constant mass  $m$  and ballistic coefficient  $\beta$  and specified cone angle and nosetip fineness ratio  $\tau$  are first considered. Then, fixed cone half-angle reentry vehicles having minimum heat transfer or truncated cone nosetips with specified  $\tau$  are considered and constrained to have constant  $m$ ,  $\beta$ , and volume  $V$ . In all cases considered, the nosetip and reentry vehicle geometry is specified a priori, the constraints are applied, but no optimization procedure is attempted. This determines the values of  $r_B$  and  $r_{\max}$  and, subsequently,  $Q$ .

Since by Eq. (4)  $Q^L$  is proportional to  $r_{\max}^{3/2}$  and according to Eq. (5)  $Q^T$  is proportional to  $r_{\max}^{9/5}$ , the total heat transfer  $Q$  may also be reduced by decreasing  $r_{\max}$ . The reduction in this case is due to the decrease in surface area of the nosetip.

Reduction in  $Q$  by reducing  $r_{\max}$  is illustrated for the selected nosetip shapes with the indicated constraints in the following subsections.

### A. SPHERE-CONE NOSETIPS, CONSTANT $m$ AND $\beta$

To illustrate the reduction in  $Q$  by means of decreasing  $r_{\max}$ , consider the following baseline sphere-cone reentry vehicle:

$$m = 400 \text{ lb}_m$$

$$\beta = 2000 \text{ lb}_m / \text{ft}^2$$

$$\theta_c = 7^\circ$$

$$r_B = 9 \text{ in.}$$

$$r_N = 2.56 \text{ in.}, r_{\max} = 2.61$$

$$\tau_{\text{nosetip}} = 2 r_{\max} / L = 2.0.$$

Our present objective is to reduce  $r_{\max}$  so as to reduce  $Q$ , but to do so maintaining  $m$  and  $\beta$  constant. Numerically calculated results<sup>5, 13</sup> satisfying the required constraints are shown in Fig. 5 and its inserted table. The reentry vehicle base radius and mass  $r_B$  and  $m$ , the ballistic coefficient  $\beta$ , and a drag integral  $I_D$  are related by

$$\beta = \frac{m}{4\pi r_B^2 I_D} \quad (23a)$$

$$r_B = \sqrt{\frac{m}{4\pi\beta I_D}} \quad (23b)$$

where

$$I_D = \int_0^{\bar{s}} \bar{p}_e \sin\alpha \bar{r} d\bar{s} \quad (24a)$$

$$C_D = 4I_D \quad (24b)$$

Reducing  $r_{\max}$  ( $r_N$ ) while maintaining  $\theta_c$  constant decreases the drag integral  $I_D$ . Requiring  $m$  and  $\beta$  to be constant thus means, by Eq. (23b), that the vehicle base radius must increase. This is the behavior seen for the three reentry vehicles shown in Fig. 5 and the corresponding vehicle parameters given in the inserted table.

<sup>13</sup>Inouye, M., J. V. Rakich and H. Lomax, "A Description of Numerical Methods and Computer Programs for Two-Dimensional and Axisymmetric Supersonic Flow over Blunt-Nosed and Flared Bodies," NASA TN-D-2970, August 1965.

VEHICLE NUMBER	$\tau_D$	$m$	$\beta$	$V$	$r_N$	$r_{max}$	$r_B$	$L_V$
		(lb <sub>m</sub> / m)	(lb <sub>m</sub> / ft <sup>2</sup> )	ft <sup>3</sup>	in.	in.	in.	in.
1	0.0282	400	2000	3.53	2.56	2.61	9.0	54.4
2	0.0167	400	2000	7.85	2.29	2.34	11.7	78.2
3	0.0116	400	2000	13.64	1.79	1.83	14.0	100.9

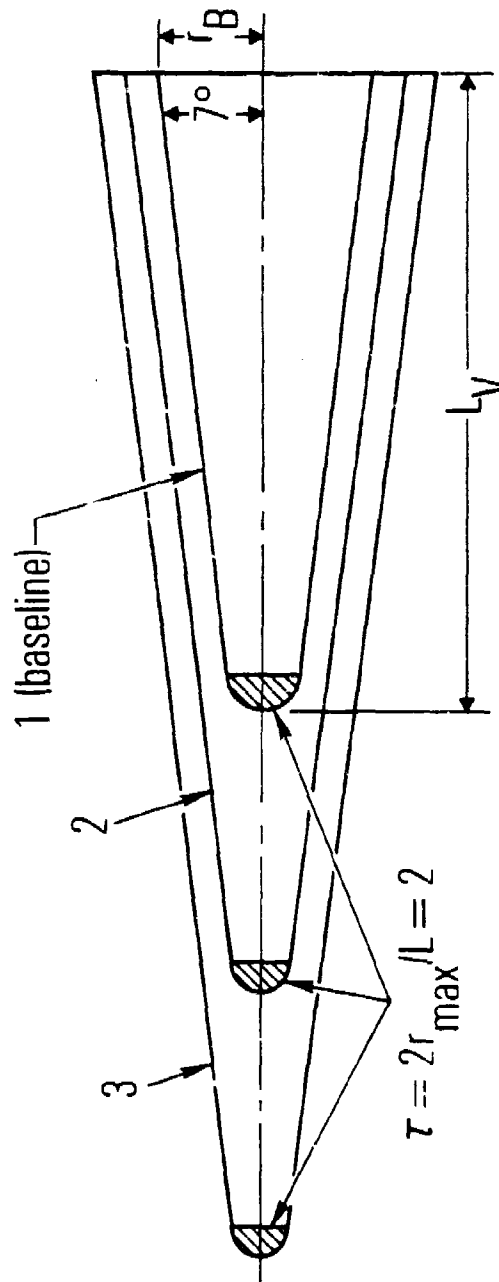
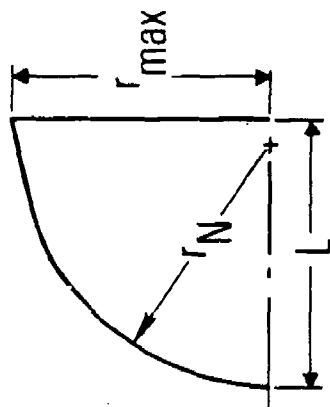


Fig. 5. Constant Ballistic Coefficient Reentry Vehicles

Since all other factors are constant, the nosetip total heat transfer  $Q$  for these three vehicles is simply proportional to a power of  $r_{\max}$ , i. e.

$$\frac{Q_3^L}{Q_1^L} = \left(\frac{1.83}{2.61}\right)^{3/2} = 0.687; \quad \frac{Q_3^T}{Q_1^T} = \left(\frac{1.83}{2.61}\right)^{9/5} = 0.528$$

$$\frac{Q_2^L}{Q_1^L} = \left(\frac{2.34}{2.61}\right)^{3/2} = 0.849; \quad \frac{Q_2^T}{Q_1^T} = \left(\frac{2.34}{2.61}\right)^{9/5} = 0.822$$

The maximum reduction in nosetip total heat transfer of 47.2% is obtained at the expense of an enormous increase in the volume and surface area of the reentry vehicle. In many instances, such increases will not be tolerable in view of volume and heat shield weight requirements.

B. MINIMUM HEAT TRANSFER NOSETIPS,  
CONSTANT  $m$ ,  $\beta$ , AND  $V$

The interaction of nosetip shape with reentry vehicle characteristics and performance is considered below for the case of minimum heat transfer nosetips on conical reentry vehicles. Since volume increases, such as those encountered in the sphere-cone geometry results just discussed, are undesirable, this additional constraint will also now be considered.

The volume of an axisymmetric reentry vehicle can be defined in terms of a volume integral  $I_V$  and the base radius  $r_B$  by<sup>2</sup>

$$V = \pi \int_0^{L_V} r^2 dz = \pi r_B^3 I_V \quad (25a)$$

where  $I_V$  is given by

$$I_V = \int_0^{2/\pi_B} \left(\frac{r}{r_B}\right)^2 \left(\frac{dz}{r_B}\right), \quad \tau_B = 2r_B/L_V \quad (25b)$$

and from this we can write

$$r_B = \sqrt[3]{\frac{V}{\pi I_V}} \quad (25c)$$

If we require a reentry vehicle to simultaneously satisfy a ballistic coefficient constraint and a volume constraint, then equating the base radius expressions given by Eqs. (23b) and (25c) gives the following required relationship between  $m$ ,  $\beta$ ,  $V$ ,  $I_D$ , and  $I_V$

$$\phi = \frac{(m/\beta)^{1/2}}{V^{1/3}} = 2.42 \frac{I_D^{1/2}}{I_V^{1/3}} \quad (26)$$

The calculated value of this dimensionless parameter for the baseline vehicle considered in Subsection V-A is 0.293. Our present objective is to determine the nosetip total heat transfer for a  $\tau = 2$  minimum turbulent heat transfer nosetip on a  $7^\circ$  conical reentry vehicle for which the  $m$ ,  $\beta$ , and  $V$  are the same as for the baseline sphere-cone vehicle.

For specified nosetip and conical afterbody geometry,  $\phi$  can easily be determined in the same manner as the integrals  $I_Q^L$  and  $I_Q^T$ , i.e., using numerically calculated values of  $\bar{p}_e$  to evaluate  $I_D$  as given by Eq. (24a) and Eq. (25n) to evaluate  $I_V$ . When this is done for the present geometry, it is found that for

$$\phi = 0.293; \quad \frac{r_{\max}}{r_B} = 0.260 \quad (27)$$

The corresponding value of  $r_{\max}/r_B$  for the baseline sphere-cone vehicle is 0.287.

Designating the sphere-cone reentry vehicle as 1 and the minimum heat transfer nosetip vehicle as 2, we also have for fixed  $\beta$  and  $m$  from Eq. (23b) and the calculated integrals  $I_D$

$$\frac{(r_B)_2}{(r_B)_1} = \frac{(I_D)_1^{1/2}}{(I_D)_2^{1/2}} = 0.998 \quad (28)$$

Thus, combining these relationships

$$\frac{(r_{\max})_2}{(r_{\max})_1} = \frac{(r_{\max}/r_B)_2}{(r_{\max}/r_B)_1} \frac{(I_D)_1^{1/2}}{(I_D)_2^{1/2}} = 0.904 \quad (29)$$

and, finally, making use of Eq. (5) and Table 1

$$\frac{Q_2^T}{Q_1^T} = \left[ \frac{(r_{\max})_2}{(r_{\max})_1} \right]^{9/5} \left[ \frac{(I_Q)_2^T}{(I_Q)_1^T} \right]^{4/5} = 0.698 \quad (30)$$

Thus, the nosetip total turbulent heat transfer is reduced 30.2%, even though the reentry vehicle volume is held constant along with the mass and ballistic coefficient. The main reason this can be done is the intrinsically higher drag coefficients for reentry vehicles with minimum heat transfer nosetips.

The basic quantity, in addition to  $I_Q$ , needed to compare nosetip ( $\tau = 2$ ) total heat transfer as in Eqs. (29) and (30) is  $(r_{\max}/r_B)/(I_D)^{1/2}$ . This parameter is shown for  $5^\circ$ ,  $7^\circ$ , and  $9^\circ$  conical reentry vehicles with  $\tau = 2$  minimum turbulent heat transfer nosetips in Fig. 6. The corresponding results for  $5^\circ$ ,  $7^\circ$ , and  $9^\circ$  conical reentry vehicles with  $\tau = 2$  sphere-cone nosetips are also shown. The baseline vehicle and the minimum heat transfer nosetip vehicle discussed above are indicated by an "x" on the  $7^\circ$  curves.

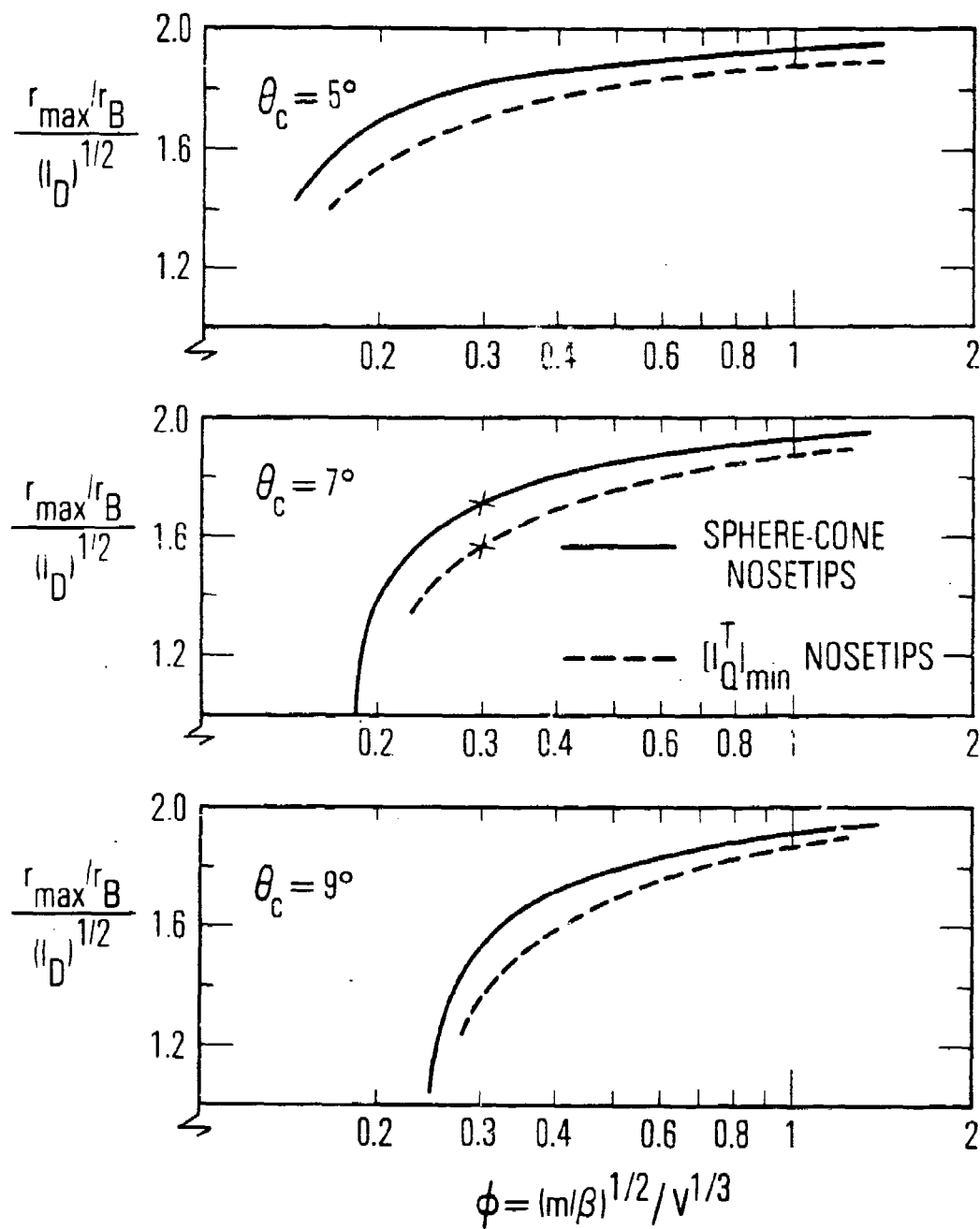


Fig. 6. Noisetip Scaling Parameter for Sphere-cone and  $[I_Q^T]_{\min}$   $\tau = 2$  Nosetips

Using Fig. 6, comparisons such as that made above can easily be made for a wide range of reentry vehicle parameters. The correlating parameter is  $\phi = (m/\beta)^{1/2}/V^{1/3}$ .

C. TRUNCATED-CONE NOSETIPS,  
CONSTANT  $m$ ,  $\beta$ , AND  $V$

From the above results, the desirability of a "high drag" nosetip for the present purpose of reducing nosetip total heat transfer can be seen. An obvious new objective thus becomes finding a nosetip shape which has large drag (high  $I_D$ ) and low heat transfer (small  $I_Q$ ). Comparison of these quantities for truncated cone nosetips, minimum heat transfer nosetips, and sphere-cone nosetips is shown in Table 2. Comparison of corresponding quantities for minimum heat transfer nosetip shapes and truncated cones indicates that the latter  $I_Q$  values are only 2 to 3% greater, whereas the latter  $I_D$  values are 28-47% greater for  $\tau \geq 2$ .

This means that using a truncated cone nosetip in place of a sphere-cone nosetip and maintaining constant  $m$ ,  $\beta$ , and  $V$ , as before, could potentially give even larger reductions in  $Q$  than using the previously determined minimum heat transfer nosetip shapes. The quantity  $(r_{\max}/r_B)/I_D^{1/2}$  for  $5^\circ$ ,  $7^\circ$ , and  $9^\circ$  conical reentry vehicles with  $5^\circ$ ,  $7^\circ$ , and  $9^\circ$  truncated cone nosetips, respectively, is shown as a function of  $\phi$  in Fig. 7.

For the  $7^\circ$  vehicles marked by the small "x" on the  $7^\circ$  curves, the truncated cone nosetip total turbulent heat transfer is 57.9% of that for the reference  $7^\circ$  sphere-cone vehicle having the same  $m$ ,  $\beta$ , and  $V$ . Recall that the corresponding reduction employing a minimum heat transfer nosetip was to 69.8% of the sphere-cone nosetip value. These results do not negate the minimum heat transfer shape results determined earlier. The minimum heat transfer shapes minimize  $Q(I_Q)$  for fixed  $\beta$  and  $r_{\max}$  as seen in Table 2. For fixed  $m$ ,  $\beta$ , and  $V$ , truncated cone nosetips allow a greater reduction in  $r_{\max}$  (because they have larger  $I_D$  values); this results in a greater reduction in  $Q$  by Eq. (5) even though  $I_Q$  for these nosetips is slightly larger than for the minimum turbulent heat transfer shapes.

Table 2. Calculated Nosedip Heat Transfer and Drag Integrals

$\tau$	Sphere-Cones			Minimum Heat Transfer				Truncated Cones					
	$\theta_c$	$i_Q^L$	$i_Q^T$	Laminar		Turbulent		$i_Q^L$	$i_Q^T$	$i_D$			
				$i_Q^L$	$i_D$	$i_Q^L$	$i_D$						
1	$5^\circ$	0.0784	0.0999		0.209						0.0845	0.0974	0.525
	$7^\circ$	0.0729	0.0941	0.0544	0.0912	0.0686	0.116				0.0772	0.0910	0.290
	$9^\circ$	0.0667	0.0883		0.172						0.0704	0.0859	0.234
2		0.0714	0.0948		0.252						0.0677	0.0770	0.392
		0.0730	0.0935	0.0612	0.227	0.0750	0.207				0.0666	0.0766	0.366
		0.0725	0.0930		0.247						0.0658	0.0765	0.341
4		0.0724	0.0903		0.348						0.0510	0.0594	0.427
		0.0724	0.0903	0.0510	0.313	0.0594	0.411				0.0510	0.0594	0.413
		0.0724	0.0903		0.348						0.0514	0.0600	0.399
8		0.0550	0.0631		-----						0.0422	0.0500	0.444
		0.0550	0.0631	0.0422	0.0433	0.0500	0.413				0.0422	0.0500	0.437
		0.0550	0.0631		-----						0.0422	0.0501	0.430

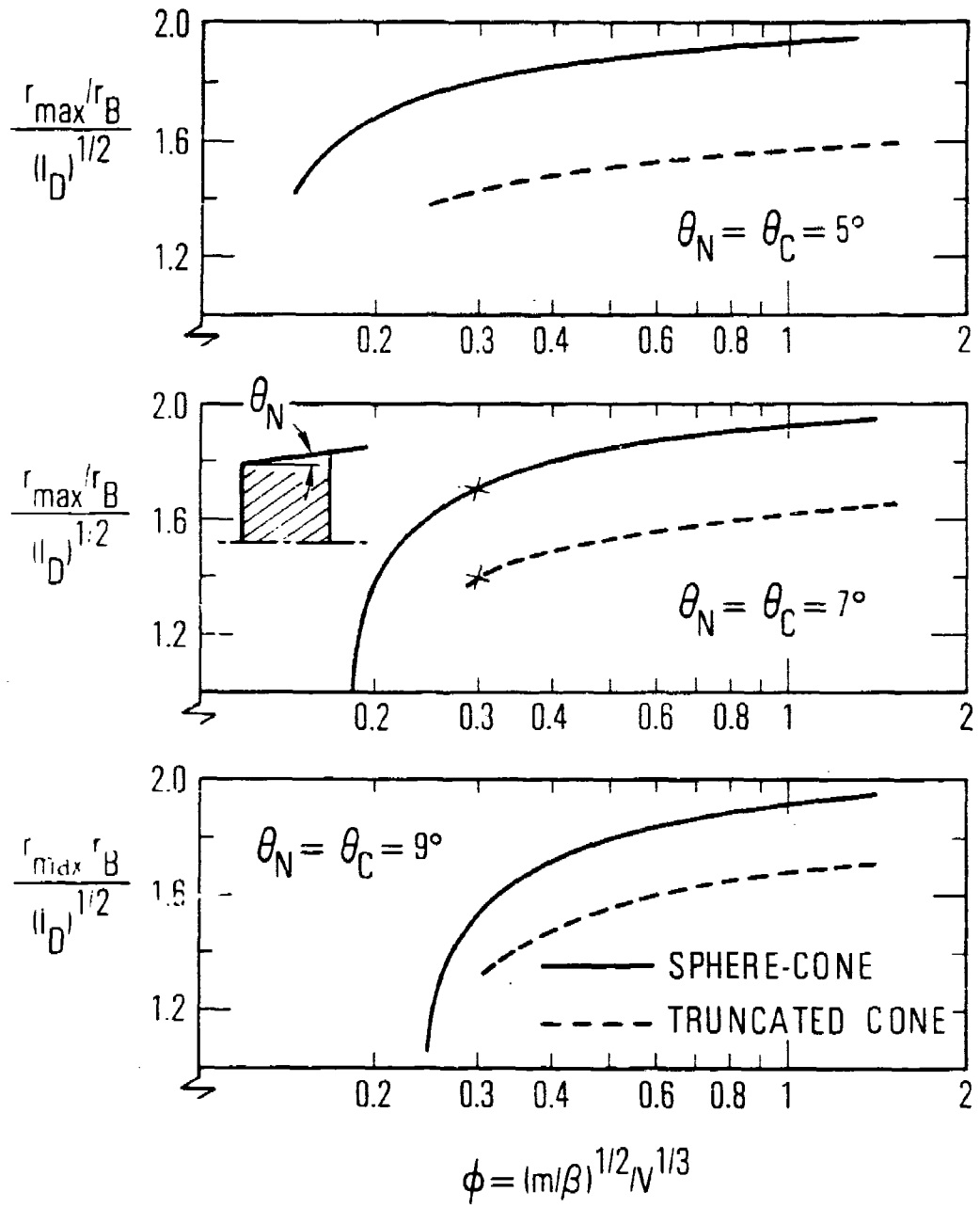


Fig. 7. Noisetip Scaling Parameter for Sphere-cone and Truncated Cone  $\tau = 2$  Noisetips

Many comparisons can be made using the results given in Figs. 6 and 7 in the manner illustrated herein. In general, the magnitude of the potential reduction in  $Q$  appears to achieve a maximum at a value of  $\phi$  which increases as the cone half-angle  $\theta_c$  increases. The maximum reduction for truncated cone nosetips ( $\tau = 2$ ) approaches 50%. It is very likely that reductions greater than this could be achieved by simultaneously optimizing both the nosetip and the reentry vehicle shape with full consideration of their interaction.

Fixed-shape flat-faced nosetips, such as those considered in this study, may possess other advantages for reentry vehicle applications in addition to reducing nosetip total heat transfer. They may significantly reduce the nosetip boundary layer transition altitude.<sup>14</sup> In addition, the rapid recompression occurring on the nosetip surface, just after the overexpansion at the flat-face corner, could possibly serve as a very effective adverse pressure gradient boundary layer trip for frustum transition. This might assure uniform movement of the frustum transition front location to the nosetip region. This becomes potentially even more attractive when coupled with significant reduction in the boundary layer unit Reynolds number on the rear portion of the reentry vehicle frustum due to the flat-nose shape.

---

<sup>14</sup> Auerbach, I., "Influence of Nosetip Shape on Boundary Layer Transition in Arc Heated Jets," AIAA Paper 78-235, AIAA 16th Aerospace Sciences Meeting, Huntsville, Ala., January 1978.

## VI. SUMMARY AND CONCLUSIONS

Flat-face nosetip shape contours that minimize reentry trajectory total nosetip heat transfer for fixed vehicle ballistic coefficient, nosetip fineness ratio, and scale have been determined using a direct optimization approach. The method utilized relies upon analytic expressions for the total integrated heat transfer to a nosetip for a constant ballistic coefficient reentry trajectory. These expressions are based upon the use of boundary layer integral heat transfer prediction methods. The surface pressure distributions, required to evaluate the heat transfer and drag functions, have been determined numerically from accurate inviscid flow field computer codes.

Minimum heat transfer flat-faced shapes have been found for fineness ratios of 1, 2, 4, and 8. The flat-face height, for both the laminar and turbulent solutions, decreases as the fineness ratio decreases. These shapes are qualitatively similar to those obtained earlier using Newtonian flow field approximations. However, the potential reduction in total heat transfer through the use of minimum heat transfer nosetip shapes in place of the normal sphere-cone geometry is much less than predicted earlier. The maximum heat transfer reduction due to nosetip shaping alone, i. e., fixed nosetip scale, is about 30%.

The optimization problem solved to determine the minimum heat transfer shapes neglects the interaction of the nosetip shape with reentry vehicle performance characteristics. The use of minimum heat transfer and truncated cone nosetips on conical reentry vehicles with this interaction considered has also been investigated. Because these shapes are high drag-low heat transfer configurations, additional decreases in nosetip total heat transfer can be realized due to the reduced scale of the required nosetip in comparison to that for a sphere-cone nosetip on a reentry vehicle having the same mass, ballistic coefficient, and volume. No attempt to optimize the nosetip shape for these additional constraints was made.

Total heat transfer reductions, with these new constraints, of 40% are possible using the previously defined  $\tau = 2$  minimum heat transfer nosetip shapes, and reductions approaching 50% are possible using the higher drag  $\tau = 2$  truncated cone nosetip shapes. Scaling relationships have been derived and presented which allow the total trajectory nosetip heat transfer for these nosetip shapes to be easily related to that for sphere-cone nosetips on conical reentry vehicles constrained to have the same mass, ballistic coefficient, and volume.